

Quantum Coherence between High Spin Superposition States of Single Molecule Magnet Ni₄

E. del Barco¹, A. D. Kent¹, E. C. Yang² and D. N. Hendrickson²

¹*Department of Physics, New York University, 4 Washington Place, New York, NY 10003 and*

²*Department of Chemistry and Biochemistry, University of California San Diego - La Jolla, CA 92093-0358*

(Dated: May 23, 2018)

Magnetic quantum tunneling in a single molecule magnet (SMM) has been studied in experiments that combine microwave spectroscopy with high sensitivity magnetic measurements. By monitoring spin-state populations in the presence of microwave magnetic fields, the energy splittings between low lying high spin superposition states of SMM Ni₄ ($S = 4$) have been measured. Absorption linewidths give an upper bound on the rate of decoherence. Pulsed microwave experiments provide a direct measure of the spin-lattice relaxation time, which is found to be remarkably long (\sim sec) and to increase with the energy splitting.

PACS numbers: 75.45.+j, 75.50.Tt, 75.60.Lr

Magnetic quantum tunneling (MQT) in single molecule magnets enables the creation of coherent high spin superposition states, which are both of great fundamental interest and essential for the use of SMMs in quantum computing [1, 2]. The main focus of experiments conducted to date, however, have been on incoherent MQT, where these superposition states are subject to rapid decay into their classical counterparts: spin-up and spin-down states [3, 4]. Decoherence generally occurs when discrete levels are coupled to an environment with many degrees of freedom, such as the modes of a lattice (phonons), the electromagnetic field (photons) or nuclear spins [5, 6, 7]. Here we investigate coherent MQT in a SMM in which the tunneling rate is faster than the rate of decoherence and at a temperature at which tunneling occurs only between the lowest lying spin states. Our experiments combine microwave excitations with high sensitivity magnetic measurements and enable continuous monitoring of spin state populations during the application of microwave radiation. Pulsed microwave experiments provide a direct measure of the spin-lattice relaxation time. Further, the linewidths associated with microwave absorption provide an upper bound on the decoherence rate of a high spin superposition state in a SMM.

We have chosen to study [Ni(hmp)(t-BuEtOH)Cl]₄, henceforth referred to as Ni₄, because this is a particularly clean SMM, with no nuclear spins on the transition metal sites [8]. The molecule core consists of four Ni^{II} (Spin 1) magnetic ions and oxygen atoms at alternating corners of a distorted cube, with S₄ site symmetry. Ferromagnetic exchange interactions between the Ni^{II} ions lead to an $S = 4$ ground state at low temperature, as determined by magnetic susceptibility measurements and high frequency Electron Paramagnetic Resonance (EPR) [8]. Magnetic hysteresis is observed below a characteristic blocking temperature (1 K) and is associated with the presence of a uniaxial magnetic anisotropy that favors high spin projections on the easy axis of the molecule, which we denote the z-axis. This uniaxial anisotropy leads to large energy barrier ($DS^2 \sim 12$ K) to magneti-

zation reversal (see Fig. 1A).

MQT is characterized by the spin Hamiltonian:

$$\mathcal{H} = -DS_z^2 - \mu_B \vec{S} \cdot \hat{g} \cdot \vec{H} \quad (1)$$

where the first term is the uniaxial anisotropy and the second term is the Zeeman energy associated with the interaction between the spin and magnetic field. An external magnetic field applied along the easy axis of the molecules H_z , tilts the double potential well favoring those spin projections aligned with the field. Note that in zero magnetic field the $|up\rangle$ and $|down\rangle$ spin-projections have nearly the same energy and MQT is possible. Importantly, in this case, a magnetic field transverse to the anisotropy axis (in the $x - y$ plane) lifts the degeneracy of these states by an energy Δ , the tunnel splitting, and leads to states that are coherent superpositions of the original $|up\rangle$ and $|down\rangle$ spin-projections. The frequency of MQT between $|up\rangle$ and $|down\rangle$ states is proportional to the tunnel splitting ($f = \Delta/h$). Fig. 1C shows the energy of the lowest lying states as a function of longitudinal magnetic field. At zero field the states are superpositions of opposite spin-projections

$$\begin{aligned} |S\rangle &= \frac{1}{\sqrt{2}}(|up\rangle + |down\rangle) \\ |A\rangle &= \frac{1}{\sqrt{2}}(|up\rangle - |down\rangle) \end{aligned} \quad (2)$$

where

$$\begin{aligned} |up\rangle &= \frac{1}{\sqrt{2}} \sum_m (a_m + b_m) |m\rangle \\ |down\rangle &= -\frac{1}{\sqrt{2}} \sum_m (a_m - b_m) |m\rangle \end{aligned} \quad (3)$$

The value of the coefficients a_m and b_m depend on the applied field. Only the coefficients with $|m| = 4$ are non-zero at zero field and the two lowest levels are $|S\rangle = \frac{1}{\sqrt{2}}(|+4\rangle + |-4\rangle)$ and $|A\rangle = \frac{1}{\sqrt{2}}(|+4\rangle - |-4\rangle)$. In the presence of a transverse magnetic field the $|up\rangle$ and $|down\rangle$ states are tilted away from the z-axis but are still separated by a large angle (see Figs. 1B and 1C), when this field is less than the anisotropy field $H_a = 2DS/(g\mu_B) = 4.5$ T.

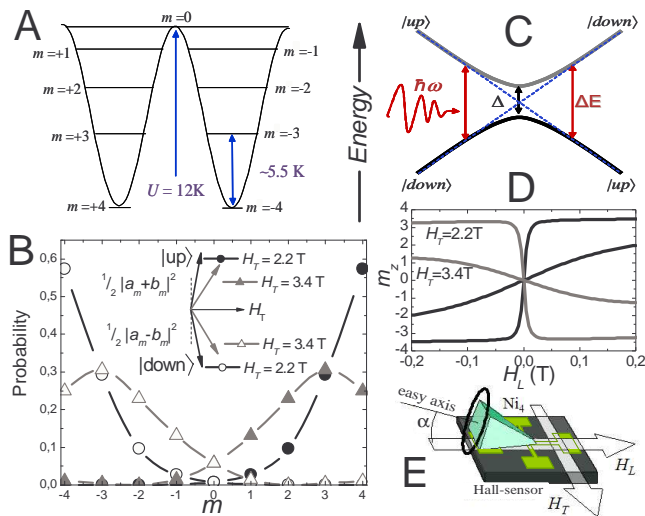


FIG. 1: (Color on-line) A) Magnetic energy levels of Ni_4 , with different z -axis spin projections labeled. B) The $|up\rangle$ and $|down\rangle$ state probability amplitudes versus z -axis projection for different transverse magnetic fields. C) Energy of the lowest lying levels in the vicinity of zero field. D) Magnetization of lowest (black) and first excited states (gray) as a function of the longitudinal field for two different transverse fields. E) Experimental configuration.

The interaction of the spin with the environment limits the coherence time of the superposition. A transverse field can be used to increase the tunnel splitting and access a regime in which the dynamics is expected to be coherent [6, 7]. It is straightforward to show that the tunnel splitting depends on the transverse field to a high power, $\sim D(H_T/H_a)^{2S}$ [9]. This enables large variations in the magnitude of the tunnel splitting for small changes in the transverse field. Fig. 1D shows the z -component of magnetization for symmetric and antisymmetric states as a function of the longitudinal magnetic field. Photon induced transitions (PIT) between symmetric and antisymmetric states produce changes of the z component of magnetization when the longitudinal field is non-zero. When the microwave field, H_{ac} , is parallel to the easy axis the transition rate is given by the following expression:

$$\Gamma = \frac{\pi}{2} \left(\frac{g\mu_B}{\hbar} H_{ac} \right)^2 |\langle S|S_z|A \rangle|^2 f(\omega) \quad (4)$$

where $\langle S|S_z|A \rangle$ is the matrix element coupling the symmetric and antisymmetric states. $f(\omega)$ is a Lorentzian which characterizes the linewidth of the resonance:

$$f(\omega) = \frac{1}{\pi} \frac{\tau_2}{1 + (\omega - \omega_0)^2 \tau_2^2} \quad (5)$$

where $\omega_0 = E/\hbar$, and E is the energy level separation. τ_2 is the transverse relaxation time or decoherence time, which sets the width of the resonance. Note that the transition matrix element is maximum at zero magnetic field, when the states are symmetric and antisymmetric superpositions of $|up\rangle$ and $|down\rangle$ states. The matrix

element decreases with longitudinal magnetic field and approaches zero when $2g\mu_B H \gg \Delta$, and states are simple up and down spin projections.

We have conducted experiments in a low temperature limit, $k_B T < E$, in which there is a significant difference in the population between the two lowest lying spin levels. A high sensitivity micro-Hall magnetometer is used to measure the z component of magnetization of a millimeter-sized single crystal of Ni_4 that is placed with one of its faces parallel to the plane of the Hall-sensor [10] (see fig. 1E). The experiments were conducted at 0.38 K in a He^3 cryostat that incorporates a 3D vector superconducting magnet, in which magnetic fields can be applied at arbitrary directions with respect to the axes of a crystal. A thin circular superconducting loop ($\phi = 2$ mm) is placed with its plane perpendicular to the easy anisotropy axis of the crystal (see Fig. 1E). This loop shorts the end of a 2.4 mm coaxial line. A 50 GHz Vector Network Analyzer is used to apply microwave radiation and enables characterization of the resonances of the loop. All the measurements were performed at loop resonances to maximize the power that is converted into ac magnetic field at the sample position. Further, pulsed microwave experiments were conducted using a pulse pattern generator to gate the microwave source.

Figure 2A shows a magnetization curve recorded in the presence of continuous-wave (CW) radiation at 39.8 GHz while a transverse field of 3.2 T was applied. Peaks and dips are observed at opposite polarities of the longitudinal field demonstrating PITs between magnetic states of the molecules with opposite spin-projections. Note that at PITs the sample temperature increases by less than 0.01 K, showing that these features are not due to sample heating. A careful inspection of the peaks shows a more complex structure: each peak is formed by two peaks, labeled A and B . Measurements carried out at lower sweep rates show that peak B is also composed of two peaks, B_1 and B_2 (see Figs. 3 and 4). This is in agreement with longitudinal field EPR experiments, where different absorption lines have been found and ascribed to molecules with slightly different values of the axial anisotropy parameter [11]. The inset of Fig. 2A shows the difference between the magnetization measured with and without microwave radiation, $M - M_{eq}$, versus field, for frequencies from 18 to 50 GHz and $H_T = 3.2$ T.

Classically the energy of these states would depend linearly on magnetic field and simply cross at zero field. However, the position of the peaks as a function of frequency does not depend linearly on magnetic field, particularly near zero longitudinal field. This is evident in Fig. 2B, which shows the position of peak A versus longitudinal field at different frequencies and as a function of the transverse field (2.2 to 3.6 T). The curvature of the energy splitting as the longitudinal field goes to zero is evidence of level repulsion and, with the measured magnetization changes, is a *clear signature of quantum superposition states with opposite magnetizations*. The solid lines are fits of the data by direct diagonalization of the Hamil-

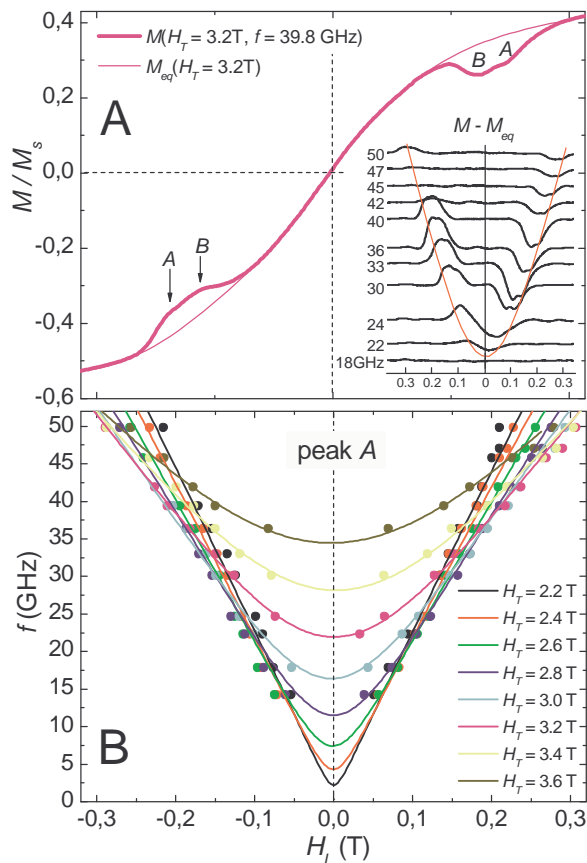


FIG. 2: (Color on-line) A) Magnetization versus longitudinal field in the presence of a transverse field, $H_T = 3.2$ T, while CW radiation of 39.8 GHz was applied. The inset shows $M - M_{eq}$ versus longitudinal field at different microwave frequencies. B) Field positions of the PITs of species A for several microwave frequencies and transverse fields.

tonian of Eq. (1) using $D_A = 0.765$ K, $B = 7.9 \times 10^{-3}$ K, $C = 3.25 \times 10^{-5}$ K, $g_z = 2.3$, $g_x = g_y = 2.23$ [12]. The behavior of the B-peaks can be fit with parameters $D_{B1} = 0.735$ K and $D_{B2} = 0.745$ K (not shown). These values are in excellent agreement with those determined from high frequency EPR experiments [11].

In order to study the dynamics of the magnetization in the presence of radiation, we have conducted experiments with pulsed microwave radiation, in which the pulse time is of the order of the longitudinal relaxation time (\sim sec). We sweep the applied longitudinal magnetic field at a rate of 8.3×10^{-5} T/s with $H_T = 3.2$ T around the position of a PIT. During this field sweep we apply pulses of 39.4 GHz with a 50% duty cycle and pulse times from 1 to 50 s. The results are shown in Fig. 3A. For the smallest sweep rate used in this experiment, 8×10^{-5} T/s, the field-width of the pulse is only 0.004 T (comparable to the size of the dots). This indicates that inhomogeneous broadening is not a significant component of the linewidth. The ratio between the magnetization when the radiation is OFF (solid circles) and ON (open circles) depends exponentially on the pulse width (Fig. 3B), $M_{OFF}/M_{ON} = \exp(-\tau/\tau_1)$. A fit to

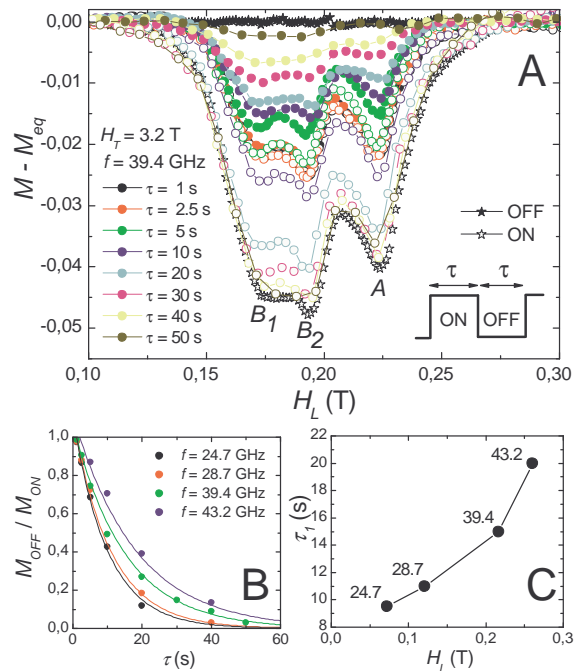


FIG. 3: (Color on-line) A) Pulsed microwave results: 50% duty cycle pulses of 39.4 GHz radiation are applied while sweeping the longitudinal field across a PIT. The transverse field is 3.2 T. The magnetization was recorded while the pulse is ON (open circles) and OFF (close circles), for pulse widths from 1 to 50 seconds. The black curves were measured with 99.99% (open black stars) and 0.01% (close black stars) duty cycles. B) The ratio between M_{OFF} and M_{ON} for PIT A versus pulse width for four different frequencies. The lines are fits to an exponential decay with a characteristic time τ_1 . C) τ_1 as a function of the longitudinal field. A decrease of the relaxation time is observed near zero field.

this expression gives τ_1 , the longitudinal (or energy) relaxation time, which governs the spontaneous decay of the excited state population. We have repeated this experiment for frequencies between 24.7 and 43.2 GHz at the same transverse field. The corresponding relaxation curves are shown in Fig. 3B. τ_1 is plotted as a function of longitudinal field in Fig. 3C. Remarkably, the relaxation time is long and increases from 8 to 20 s as the field and thus frequency increase. This is contrary to general ideas that the relaxation time should decrease with frequency, because of the increasing phase space available for phonon generation [13, 14].

We have measured the change in magnetic response as a function of the power of the incident CW radiation (39.4 GHz) to estimate the decoherence rate. A transverse magnetic field of 3.2 T is applied and a longitudinal field is swept at a rate of 1.6×10^{-4} T/s. The microwave power at the source was varied from -20 dBm to 2.5 dBm. The normalized change in magnetization $(M - M_{eq})/M_{eq}$ is shown as a function of the longitudinal field in Fig. 4A for different microwave powers. Fig 4B shows the amplitude for peak A versus power. The maximum power applied to the sample produces transitions in 20% of the molecules [15]. Larger magnetization changes

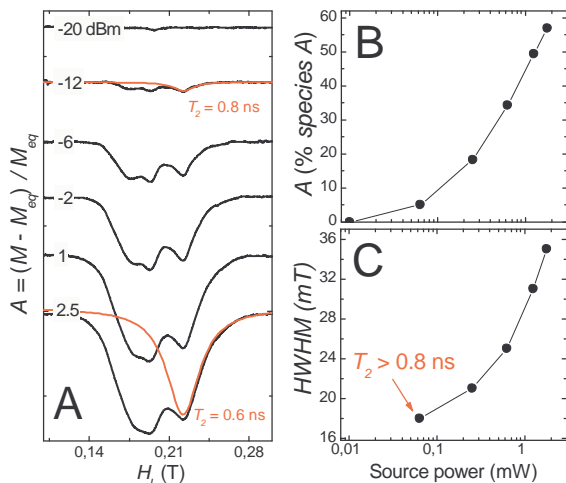


FIG. 4: (Color on-line) A) $(M - M_{eq})/M_{eq}$ for different powers with CW 39.4 GHz radiation applied to the sample. The longitudinal field was swept at 1.6×10^{-4} T/s and $H_T = 3.2$ T. Note that the curves are offset for clarity. The red lines are fits to a Lorentzian with $\tau_2 = 0.6$ ns. Figures B and C show the dependence of the amplitude and half width of PIT A, respectively.

(up to 30%) have been obtained with higher transverse fields and at lower microwave frequencies (not shown). If we consider that this amplitude corresponds to one of the peaks, which represents only a fraction of the molecules in the crystal, then the amplitude for this species is considerably larger. As an estimate, if each of the species represented one third of the total, then a net amplitude of 20% corresponds to 60% of molecules in that species. The amplitude versus power for peak A is shown in Fig. 4B (assuming a 33% population). For this curve we can estimate the power necessary to saturate the resonance. We find 50 mW (source power) in this case (and about 5 mW with $H_T = 3.4$ T and $f \sim 30$ GHz, not shown). We have fit the results shown in Fig. 4A to a Lorentzian

function $f(\omega)$ for the PIT A, as this feature is easily distinguished from the others. We find that $\tau_2 = 0.6$ ns for the curve measured with the highest power (2.5 dBm) or a resonance quality factor of ~ 10 .

In Fig. 4C we show the dependence of PIT A's half width at half maximum (HWHM) versus the microwave power at the source. The minimum width (lowest power) allows us to estimate a lower bound for the transverse relaxation time. The results from the fit of the -12 dBm curve are shown in Fig. 4A and give $\tau_2 > 0.8$ ns. The homogeneous linewidth represented by τ_2 will be less than that associated with inhomogeneous broadening. However, we note that we recover the full amplitude of the peaks and dips during the pulsed-radiation experiments (see Fig. 3A), for sufficiently long pulses ($\tau > 20$ s). This indicates that $\tau_2 \sim \tau_\phi$. A very similar decoherence time, $\tau_\phi = 1$ ns, has been recently reported in high frequency EPR experiments carried out in a single crystal of a Mn_4 SMM dimer ($S = 9/2$) [16].

This experiment demonstrates the vast difference in time scales between the longitudinal and transverse relaxations times of high spin superposition states. Clearly, for applications in quantum computing decoherence is a major challenge, which is likely amenable to synthetic strategies of nuclear isotope purification and further reduction in intermolecular interactions. Antiferromagnet molecular magnets with an uncompensated electronic or nuclear spins that tracks the Neel vector for readout are also excellent candidates for long coherence times in mesoscopic spin-systems and for use in quantum computation [17]. These will be the subject of future investigations along with studies of Rabi oscillations in molecular nanomagnets induced by shorter and higher amplitude pulsed microwave magnetic fields.

This research was supported by NSF (Grant Nos. DMR-0103290, 0114142, and 0315609).

-
- [1] A. J. Leggett, Prog. Theor. Phys. Suppl. **69**, 80 (1980).
 - [2] M. Leuenberger and D. Loss, Nature **410**, 789 (2001); J. Tejada, E. M. Chudnovsky, E. del Barco, and J. M. Hernandez, Nanotechnology **12**, 181 (2001)
 - [3] J. R. Friedman, M. P. Sarachik, J. Tejada, and R. Ziolo, Phys. Rev. Lett. **76**, 3830 (1996); J. M. Hernandez *et al.*, Europhys. Lett. **35**, 301 (1996); L. Thomas, F. Lionti, R. Ballou, D. Gatteschi, R. Sessoli and B. Barbara, Nature(London) **383**, 145 (1996).
 - [4] W. Wernsdorfer and R. Sessoli, Science **284**, 133 (1999).
 - [5] N. V. Prokof'ev and P. C. E. Stamp, Rep. Prog. Phys. **63**, 669 (2000).
 - [6] P. C. E. Stamp and I. S. Tupitsyn, Phys. Rev. **B69**, 014401 (2004).
 - [7] E. M. Chudnovsky, Phys. Rev. Lett. **92**, 120405 (2004).
 - [8] E. C. Yang *et al.*, Polyhedron **22**, 1727 (2003).
 - [9] D. A. Garanin and E. M. Chudnovsky, Phys. Rev. **B56**, 11102 (1997).
 - [10] A. D. Kent, S. von Molnar, S. Gider and D. D. Awschalom, J. Appl. Phys. **76**, 6656 (1994).
 - [11] R. S. Edwards *et al.*, J. Appl. Phys. **93**, 7807 (2003).
 - [12] There is an additional transverse anisotropy term in eqn (1) of the form $C(S+4 + S-4)$ seen in EPR studies [8, 11].
 - [13] See, for example, eqn. 26 of Ref. [7].
 - [14] N. V. Prokof'ev and P. C. E. Stamp, Phys. Rev. Lett. **80**, 5794 (1998).
 - [15] Considering the losses in the coaxial line (~ 15 dB) and the measured reflected power (~ 55 dB), we estimate that the power irradiated by the loop antenna is $P_{loop} = 0.032P_{source}$, (i.e. for $P_{source} = 2.5$ dBm = 1.77 mW the power radiated by the loop antenna is $P_{loop} \sim 50\mu\text{W}$ at 39.4 GHz). Taking into account the change in the magnetization at the PIT, we estimate that the power absorbed by the sample is 2% of the power irradiated by the loop antenna. So for $P_{loop} \sim 50\mu\text{W}$ at 39.4 GHz, the power absorbed is $\sim 1\mu\text{W}$.

[16] S. Hill, R. S. Edwards, N. Aliaga-Alcalde and G. Christou, *Science* **302**, 1015 (2003).

[17] A. Chiolero and D. Loss, *Phys. Rev. Lett* **80**, 169 (1998).